Novel membrane percrystallisation process for nickel sulphate production

Rasmus S.K. Madsen, Julius Motuzas, Anne Julbe, James Vaughan, João Diniz da Costa

Hydrometallurgy 185 (2019) 210–217

Contents lists available at ScienceDirect

Hydrometallurgy

journal homepage: www.elsevier.com/locate/hydromet

Novel membrane percrystallisation process for nickel sulphate production

Rasmus S.K. Madsen[a], Julius Motuzas[a], Anne Julbe[b], James Vaughan[c,*], João C. Diniz da Costa[a]

[a] The University of Queensland, FIM²Lab – Functional Interfacial Materials and Membrane Laboratory, School of Chemical Engineering, Brisbane, QLD 4072, Australia
[b] Institut Européen des Membranes (IEM – UMR 5635 CNRS, ENCM, UM), Université de Montpellier, CC47, Place Eugène Bataillon, 34095 Montpellier Cedex 5, France
[c] The University of Queensland, Hydrometallurgy Research Group, School of Chemical Engineering, Brisbane, QLD 4072, Australia

ARTICLE INFO

Keywords:
Nickel sulphate
Percrystallisation, inorganic carbon membrane
Carbon structure
Crystals

ABSTRACT

This research reports on an investigation of the performance of inorganic membranes for use in the percrystallisation of nickel sulphate hydrate. In this novel process, the separation of the solvent (water) and the crystallised solute (nickel sulphate hydrate) occurs continuously in a single-step, avoiding further downstream processing (crystal filtering and drying). The inorganic membranes were synthesised with sucrose solution followed by a post vacuum-assisted impregnation of the coated film on a α-alumina substrate and carbonisation under nitrogen atmosphere. The highest fluxes measured were 22 L m^{-2} h^{-1} and 1 kg m^{-2} h^{-1} (40 g L^{-1}) for water and nickel respectively. Interestingly, the transport of solution through the membrane also affected the hydration state of the nickel sulphate, as well as the crystal type and shape. High water fluxes delivered pure nickel sulphate heptahydrate with elongated and laminar crystal particles (~200 μm). Lower water fluxes produced both heptahydrate and hexahydrate salts with approximately spherical particles (also ~200 μm). There a number of factors that influence the crystallisation reaction such as the rate of evaporation which affects water availability and the resultant temperature at the permeate side of the membrane. Finally, the activation energy for nickel sulphate crystallisation was estimated to be approximately 16 kJ mol^{-1} based on feed solution temperatures.

1. Introduction

Owing to its electrochemical and electric properties (Lei et al., 2014; Xiong et al., 2015; Dimaras, 1956; Lascelles et al., 2005), nickel has been gaining increased interest from the research community. One of major applications is the incorporation of nickel in cathode (Oh et al., 2018; Zhao et al., 2018) and in perovskites for bi-functional catalytic material for lithium ion batteries (Gong et al., 2018), as connectors for current collectors (Lee et al., 2018) as well as in capacitors (Wang et al., 2018; Lamiel et al., 2017). Indeed the electronic market has spurred research into higher capacity batteries, where nickel is one of the key components. Consequently, the portable battery market has been the driving force for the ever-increased demand in nickel precursor production, which requires salts such as nickel sulphate (INSG, 2018; GME, 2015–2018). Nickel sulphate is most commonly obtained by the dissolution of nickel metal or nickel containing intermediates in a sulphuric acid solution. Subsequently, the solution is processed downstream in a crystallisation process employing solvent displacement or extraction, such as vacuum evaporation with seeding, in order to attain high-quality nickel sulphate product (Olivier et al., 2012; Moldoveanu and Demopoulos, 2002; Bamforth and Crystallizers, 1965a; Bamforth and Crystallizers, 1965b). Nickel sulphate is also produced in significant quantities as a by-product of platinum production and copper electro-refining. Nickel sulphate is highly soluble in water and its solubility was shown to have a positive correlation with temperature in water over the range of 60–80 °C and a negative correlation with sulphuric acid concentration; the temperature-solubility correlation reverses when the sulphuric acid concentration is above about 25 wt% (Havlik et al., 1996).

The crystallisation of solutes is an important industrial unit operation widely used for the production of a range of products such as sodium chloride (Varnavas and Lekkas, 1996; Hewitson, 2017), paracetamol (Prasad et al., 2000), struvite (Quist-Jensen et al., 2018) and nickel sulphate (Lascelles et al., 2005; Moldoveanu and Demopoulos, 2002) to name a few. Conventional crystallisation processes are energy intense (Hasan and Louhi-Kultanen, 2016; Semiat, 2008) and require large plant footprints (Government of South Australia, Department of the Premier and Cabinet, n.d.). Further challenges include controlling the reaction kinetics that can lead to inconsistent quality of the products (Beckmann, 2013). In recent years, research has been focused on the development of new crystallisation technologies to address the shortcomings of conventional and mature crystallisation processes. One

* Corresponding author.
E-mail address: james.vaughan@uq.edu.au (J. Vaughan).

https://doi.org/10.1016/j.hydromet.2019.02.015
Received 26 October 2018; Received in revised form 12 February 2019; Accepted 23 February 2019
Available online 02 March 2019
0304-386X/

of these technologies is membrane assisted crystallisation. To date, a range of polymeric membranes have been described for use in the crystallisation of sodium chloride, magnesium sulphate hydrate (Mariah et al., 2006), lithium chloride (Quist-Jensen et al., 2016) and sodium carbonate (Ye et al., 2013), or recovery of sodium chloride from reverse osmosis (RO) brines (Tsai et al., 2017; Ji et al., 2010), in addition to pharmaceutical products such as lysosome (Curcio et al., 2005) and protein (Polino et al., 2017).

Inorganic membrane technology has only recently been proposed for assisting crystallisation processes. In 2018, Motuzas and co-workers (Motuzas et al., 2018) pioneered a novel continuous crystallisation process which resulted in a one-step separation of solvent and dry crystals by employing an inorganic membrane. This work showed the potential of using porous carbon membranes for the production of crystals for various industrial segments such as hydrometallurgy, pharmaceutical, food and chemical industries. In a subsequent work, Madsen et al. (Madsen et al., 2018) reported that the size of the resultant sodium chloride crystals were controlled by the conditions used to prepare the porous carbon membranes and operating process conditions. For instance, average particle crystal size of 2.5 μm were obtained by inorganic membranes, much smaller by up to two orders of magnitude than those of 20–200 μm and 300–1000 μm (Ji et al., 2010; Chen et al., 2014) reported for polymeric membranes. Therefore, inorganic membranes are opening a window of research opportunities to develop new percrystallisation processes in chemical engineering and hydrometallurgical processes.

This work demonstrates for the first time the use of carbon membranes for the percrystallisation of nickel sulphate, where operation conditions affect the hydration state of the formed salt. This work also shows that membrane percrystallisation is an effective way of crystallising the solute whilst concomitantly separating the solvent (water) from the target salt in a single-step process. The effect of carbon content in the membrane and testing conditions on water and nickel fluxes were investigated. A number of characterisation techniques were used to analyse the membrane morphological features such as scanning electron microscopy and helium pycnometry. The formed crystals were also analysed by scanning electron microscopy, thermogravimetry and X-ray diffraction to determine the particle size, morphologies and the degree of hydration of the resultant salt.

2. Experimental

2.1. Membrane preparation and characterisation

Membrane coating solutions were prepared by dissolving 20, 30, 40 and 50 wt% sucrose (> 99.8% Chem-supply) into demineralised water. The solutions were mixed, followed by 30 min of sonication. Subsequently, the solutions were used to dip-coat tubular α − alumina substrates (Ceramic Oxide Fabricators, Australia). The substrates had a mean pore size of 0.1 μm, a total length of ~4 cm, external and internal diameters of 1 and 0.45 cm, respectively. Dip coating (built in house) was performed on the outer shell of the α − alumina support (Ceramic Oxide Fabricators (Aus.) Pty Ltd., Australia). Each tube was submerged in a solution for 3 min, with a submersion and withdrawal speed of ~31 cm min^{-1}. After dip coating, vacuum (< 1.3 mbar) was applied through the inner shell of the tube, causing partial impregnation of the sucrose top layer coated into the α − alumina tube. The impregnated supports were dried overnight at 60 °C before being carbonised in an inert nitrogen atmosphere at 750 °C in a tube furnace (Nabertherm) with a Eurotherm PID temperature controller. The heating and cooling ramps were 5 °C min^{-1} with a dwell time of 4 h. After carbonisation, both ends of the membrane tube were coated with Protek type N blue solvent cement to create a sealing area. The final active length of the membrane tube was ~3 cm for percrystallisation testing.

The morphology of the membranes were analysed by scanning electron microscope (SEM), using a Jeol JSM-7001F SEM with a hot (Schottky) electron gun and an acceleration voltage of 5 kV. As-prepared carbon membrane samples were crushed and annealed in air using thermogravetric analysis (TGA-DSC1 Mettler Toledo) to determine the carbon content. The heating rate was set to 10 °C min^{-1} and the maximum temperature was set to 1000 °C with a dwell time of 30 min. Pore volumes of the membranes (including substrate) were measured by an AccuPyc 1340 Gas pycnometer Micromeritics) instrument at room temperature using helium (99.995% purity). The samples were initially degassed by applying vacuum, and purged with helium before measuring the volume ten times to obtain an average value.

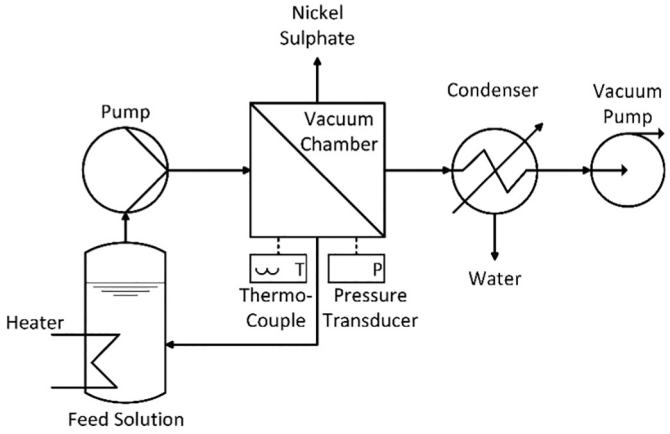

Fig. 1. Schematic of percrystallisation setup used for one-step separation of $NiSO_4$ and water.

2.2. Membrane testing and nickel sulphate characterisation

Fig. 1 shows a schematic of the membrane percrystallisation setup used in this work. Nickel sulphate solutions were prepared by dissolving amounts of $NiSO_4 \cdot 6H_2O$ (≥98% Chem-Supply) in demineralised water to acquire the desired nickel concentrations (10, 40, 70, and 100 g L^{-1}). The solutions were heated up to specific temperatures (30, 40, 50, and 60 °C) and fed through the inner shell of the membrane tube using a peristaltic pump with a flow rate of ~31 L h^{-1} to reduce potential concentration and temperature polarisation effects. A Büchner flask was utilised as a container for housing the membrane which was connected to a cold trap (submerged in liquid nitrogen), followed by an isolation valve and a vacuum pump. The percrystallised nickel sulphate crystals were collected in the Büchner flask and the solvent (water) in the cold trap. The percrystallised nickel sulphate samples were dissolved in a known volume of water to determine the solution conductivity. The fluxes were calculated by using standard curves of concentrations vs conductivity.

Percrystallised nickel sulphate samples were subsequently removed from the crystal collection chamber for further characterisation using the SEM and TGA equipment above described. In this case, TGA analysis was used to quantify the mass of dry nickel sulphate by heating the powder up to 800 °C with a heating rate of 10 °C min^{-1}. In addition, the dry powder was also studied by X-Ray Diffraction (XRD) to define the crystalline structure. XRD was carried out using a Rigaku Smartlab X-ray diffractometer at 45 kV, 200 mA, having a step increment of 0.02° and a step speed of 4°min^{-1} with filtered Cu Kα radiation (λ = 1.5418 Å).

3. Results and discussion

3.1. Membrane percrystallisation process

The transport of solute and solvent in membrane percrystallisation is schematically idealized in Fig. 2. Both water and ions permeate from the feed side (inner shell) to the permeate side (outer shell) of the

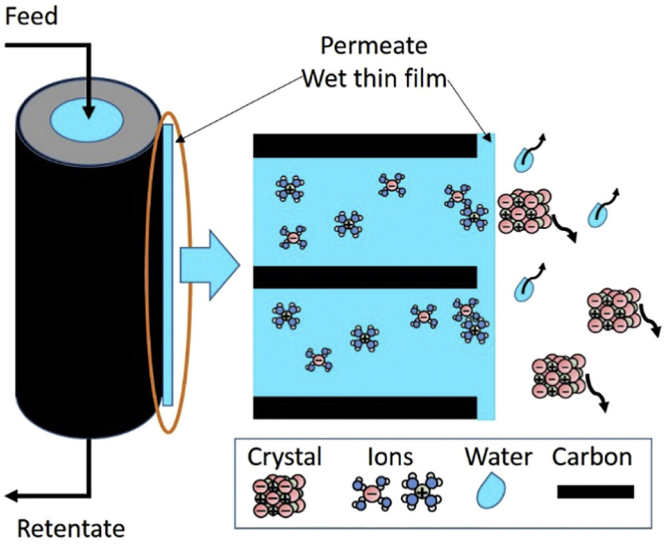

Fig. 2. Idealized illustration of the membrane percrystallisation mechanism.

membrane. The thin carbon film on the permeate side provides the ideal conditions for the formation of a wet thin film under pervaporation. Without the formation of this wet thin film, continuous percrystallisation is not attained. For instance, blank alumina substrates resulted in pore flooding as the solution fully permeates through the substrate where a wet thin film in the permeate side of the membrane cannot be formed. The wet thin film on the carbon membrane plays a fundamental role in this process. Under equilibrium conditions, the amount of water evaporating from the thin wet film is replenished by water diffusing through the membrane tube and top carbon film. As water evaporates from the wet thin film, it provides the ideal conditions for supersaturation, leading to nucleation and crystallisation of nickel sulphate hydrate. This is the reason why this novel membrane concept is called percrystallisation, where both solvent and solute permeate through the membrane, followed by crystallisation of the solute at the permeate side. The pressure difference between the feed and permeate results in continuous ejection of formed crystals from the surface of the wet thin film. The heavier crystals tend to fall to the bottom by gravity whilst the lighter solvent vapour can be recovered from the top for further re-use. This is the only membrane process that separates liquids from solids in a single-step. A video in supplementary information shows visually how the membrane percrystallisation process takes place.

In terms of chemical engineering and hydrometallurgical processes, there are many potential advantages of this novel membrane prescrystallisation process. Fig. 3 depicts the conventional membrane crystallisation and membrane percrystallisation process flow diagrams. In the case of the former, only the solvent permeates through polymeric membranes, resulting in the formation of crystals on the feed side of the membrane. These crystals subsequently require downstream processing, namely filtering and drying. In the case of membrane percrystallisation, it is a single-step process only where both solvent and solute are separated simultaneously in a single process at the permeate side of the membrane. This type of process is envisaged to deliver major operational and capital savings in crystallisation in hydrometallurgical applications, thus dispensing the need for extra costs associated with additional downstream units and thermal energy to dry crystals, in addition to effective solvent recovery.

3.2. Membrane percrystallisation characterisation and performance

Fig. 4a presents the pore volume as a function of the sucrose concentration in the solution used to prepare the membranes. The pore volume remained almost constant with a slightly decrease as the precursor solution increased in concentration, which is attributed to the increase of sucrose deposition during dip coating of the substrate. This is demonstrated by TGA results derived from the carbonisation of sucrose as shown in Fig. 4b, where mass loss increased almost linearly from 1.0 to 3.1 wt% as the sucrose concentration of the dipping solution changed from 20 to 50 wt%, respectively. This finding indicates that the changes of carbon content deposited on the $\alpha-$ alumina support was linear to the sucrose concentration.

Contrary to the α-alumina substrate that has a white colour, the dark black colour of the membranes is associated with the carbonisation of the deposited sugar solution at high temperatures. It should be noted that the dark colour is uniform throughout the membrane tubes, as previous works using other carbon precursors such as P123 (triblock *co*-polymers) in silica (Elma et al., 2015) or phenolic resin (Abd Jalil et al., 2017) have not yielded a dark colour throughout the cross section of the membrane. This observation may be directly related to the short chain of the sugar molecules in aqueous solutions used in this work, which can easily diffuse through the large pores of the α-alumina substrate via capillary forces by contact a dry solid surface to liquid solution (Kornev and Neimark, 2001). In the case of long chain carbon precursors previously reported, these tend to aggregate to form films and their diffusion is hindered throughout the α-alumina substrate. Finally, a colour gradient is observed in Fig. 4c as the membranes prepared with the lower concentration resulted in a lighter dark colour while the highest concentration yielded the darkest colour. The colour gradient is clearly associated with the mass of sugar retained during the dip coating method, which in turn is a function of the concentration of the solution as ascertained in Fig. 4a and b.

Fig. 5a shows the fluxes of water and nickel sulphate hydrate crystals produced by the membrane percrystallisation process at a feed temperature of 40 °C and a feed concentration of 40 $g\,L^{-1}$ nickel. Although the nickel crystals and solutions are indeed nickel sulphate, in this work we report their values based on the mass of nickel only, as nickel sulphate may contain different hydration states. The initial finding is that all the prepared membranes in this work were able to continuously percrystallise nickel sulphate hydrates. Further, there is a decreasing trend in both water (from 22 to 13 $L\,m^{-2}\,h^{-1}$) and nickel production (from 1.0 to 0.77 $kg\,m^{-2}\,h^{-1}$) as the sucrose solution used to prepare membranes increased in concentration. These changes equate to a 40% and 45% decrease in water percrystallised nickel fluxes, respectively. These trends are well-aligned with the pore volume as well as carbon content results in Fig. 4a and b. This finding suggests that the lower carbon content retained by the membrane prepared with 20 wt% sucrose solution delivered the best structural modulation for percrystallisation, which yielded the best permeation and evaporation performance. Fig. 4b shows the single pass percrystallisation nickel recovery ratio of 4.3%, representing the flux through the permeate over the retentate (J_{Ni} $(J_{Ni} + J_{H2O})^{-1} \times 100$). This recovery ratio can be improved by reducing the solution feed flow rate. However, in this work, a high feed flow rate was used to reduce the effects of concentration and temperature polarisation.

Fig. 6a shows the nickel and water fluxes for the carbon membrane prepared with 20 wt% sucrose solution as a function of the feed nickel solution concentration. It is observed that the water production rates decreased by 66% (from 30 to 10 $L\,m^{-2}\,h^{-1}$) as the feed concentration of nickel increased, while the opposite is true for the nickel fluxes, which increased by 373% (from 0.28 to 1.3 $kg\,m^{-2}\,h^{-1}$). The highest nickel flux is equivalent to 11,388 kg per year for 1 m^2 of membrane area, a high annual production rate. The decrease in water flux is consistent with work done on membrane distillation systems with highly concentrated solutions (Mariah et al., 2006; Tun et al., 2005). This is attributed to the decrease in the driving force, as the partial pressure of water decreases as the concentration of the nickel increases. Likewise, the increase in nickel flux is also directly associated with the driving force, as the concentration of nickel in the feed solution also

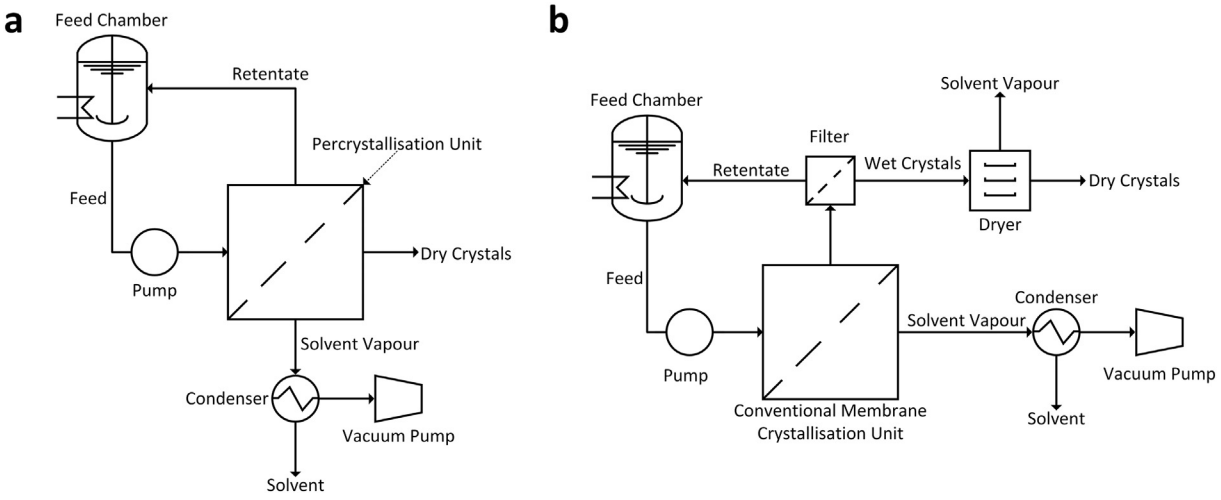

Fig. 3. Simplified process flow diagrams of (a) membrane percrystallisation and (b) membrane crystallisation.

increased. The observed plateau in the nickel flux at nickel feed concentrations of 60 mg L^{-1} is attributed to process limitations. In this case, the percrystallisation process is mainly controlled by the evaporation of water from the wet thin film as depicted in the schematic in Fig. 2. As the water evaporation is greatly reduced for high nickel feed solutions, this caused a reduction of the permeation of feed solutions through the feed side to the permeate side, thus explaining the reduction of nickel flux.

Fig. 7a presents the fluxes of nickel and water, using the best performing 20 wt% sucrose carbonised membrane, with a nickel feed concentration of 40 g L^{-1} while varying the operating temperature. A near linear trend in water and nickel production rates are observed, with water increasing by 76% (from 16 to 29 L m^{-2} h^{-1}) accompanied by nickel flux increase of 80% (from 0.73 to 1.3 kg m^{-2} h^{-1}). By increasing the temperature of the feed solution, the driving force (temperature gradient) increases. In addition, the solubility of nickel salts is also increased at the feed side of the membrane. As a result, more water is evaporated from the wet thin film and concomitantly with the solubility increase in feed side; nickel crystal flux is also increased. The recovery ratio in Fig. 7b follows a horizontal linear trend, thus indicating the theoretical recovery ratio of nickel to water in a single pass under the testing feed flow rate.

Fig. 8 shows the apparent activation energies for water of 15 kJ mol^{-1} and nickel of 16 kJ mol^{-1} required in the membrane

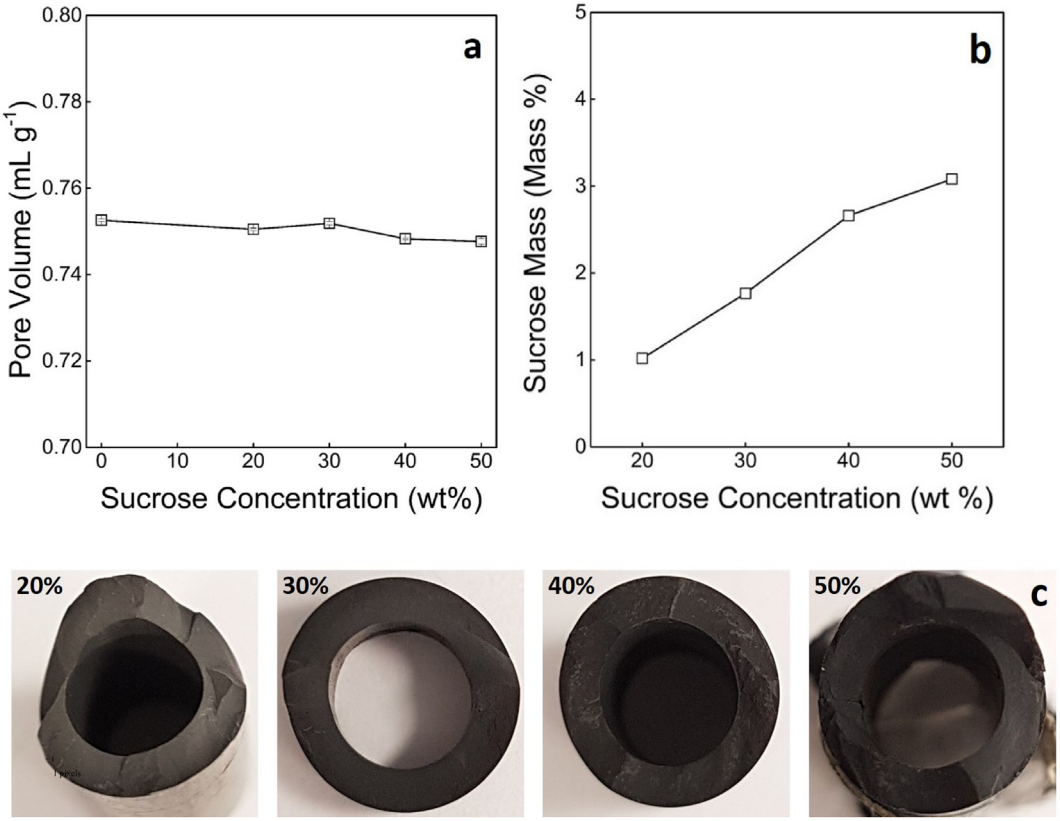

Fig. 4. (a) Pore volume in membrane material, as a function of dipping concentration; (b) carbon mass content in membrane material after carbonisation as a function of sucrose concentration used for dip coating; (c) images of the cross-section of carbonised sucrose membranes at various concentrations.

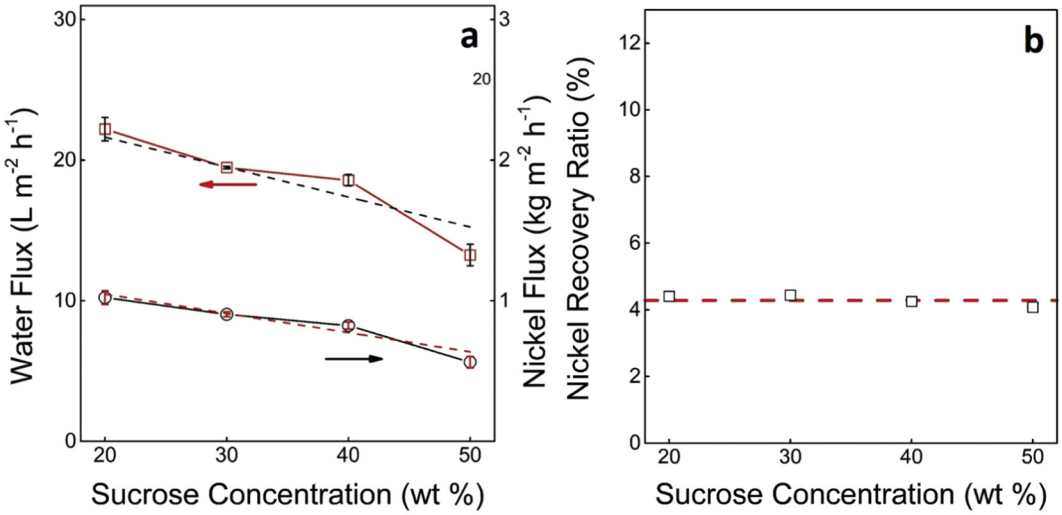

Fig. 5. (a) Water and nickel fluxes and (b) nickel single pass recovery ratio as a function of the sucrose concentration used for membrane preparation. Testing conditions were nickel feed concentration of 40 g L^{-1} and a temperature of 40 °C.

percrystallisation process. These values were calculated based on an Arrhenius-type equation using the natural logarithm to the flux over the feed temperature. The apparent energy of activation for both evaporation of water and percrystallisation of nickel sulphate were both found to be in the range of diffusion-controlled reactions in water (Su and Puls, 1999; Mortimer et al., 2002; Pilling and Seakins, 1999). The apparent activation energy for the flux of water (15 kJ mol^{-1}) is comparatively lower than what is found in work investigating pervaporation and membrane distillation processes which is reported to be in the range of 15 to above 50 kJ mol^{-1} (Feng and Huang, 1996; Sarti et al., 1985; Peng et al., 2005; Huang et al., 2014; Liang et al., 2015; Weschenfelder et al., 2015; Xu et al., 2016; Zhang and Wang, 2016). This means that the energy barrier for water flux in membrane percrystallisation is lower. Water evaporation from the wet thin film is a paramount aspect of membrane percrystallisation, in turn controlling the nickel fluxes. Hence, the lower apparent activation energy of water fluxes are also accompanied by lower apparent activation energy of nickel fluxes. In other words, membrane percrystallisation requires less energy to crystallise nickel sulphate compared to other crystallisation processes such as laboratory-scale fluidised-bed crystallisers, with an apparent activation energy calculated of 70.5 kJ mol^{-1} (Phillips and Epstein, 1974).

3.3. Nickel sulphate hydrate characterisation and discussion

The produced nickel sulphate particles were analysed by XRD, where the diffraction patterns of the obtained samples are given in Fig. 9. A key observation from the XRD patterns is that the solutes produced by the carbon membranes derived from 40 wt% and 50 wt% sucrose solutions, or using high feed concentration of 100 g L^{-1}, exhibited diffraction peaks consistent with nickel sulphate hexahydrate and heptahydrate. In all the other samples only the peaks assigned to nickel sulphate heptahydrate were detected. These results indicated that there is a relationship between the resultant crystal structure and the transport properties of the membranes.

The formation of different crystalline phases is related to the mechanism of membrane percrystallisation in Fig. 2, in particular by the role of the wet thin film in the evaporation of the solvent (water). The solvent evaporation rate is modulated by the flow of solution from the feed to the permeate surface of the membrane which is critical in the formation of solute crystals. A detectable amount of hexahydrate crystals was obtained by the membranes prepared with higher sucrose

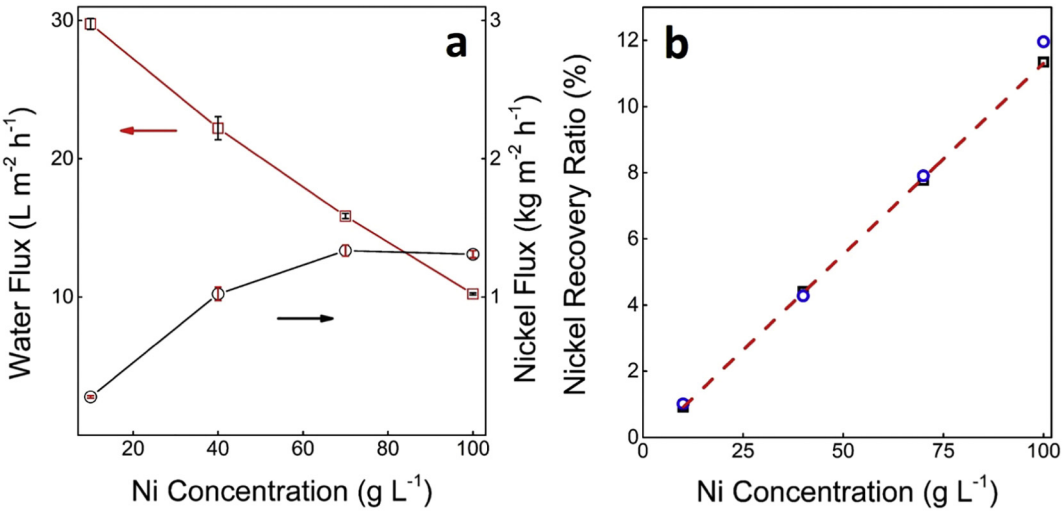

Fig. 6. (a) Water and nickel fluxes and (b) nickel recovery ratio as a function of nickel feed concentration. Testing conditions included a membrane dip-coated in 20 wt% sucrose solution concentration at a temperature of 40 °C.

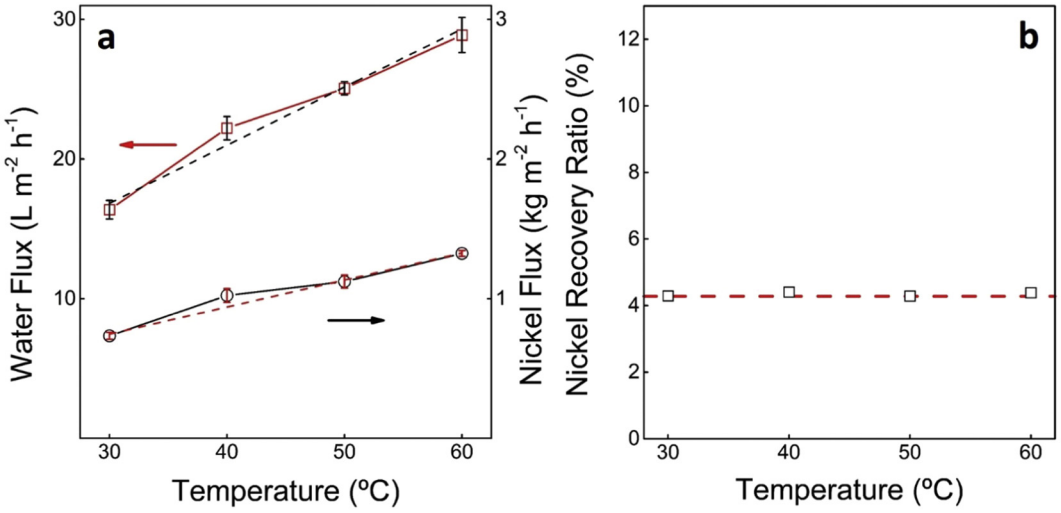

Fig. 7. (a) Water and nickel fluxes and (b) nickel recovery ratio as a function of operating temperature. Testing conditions included using a carbon membrane dip coated in 20 wt% sucrose solution and a feed nickel concentration of 40 g L^{-1}.

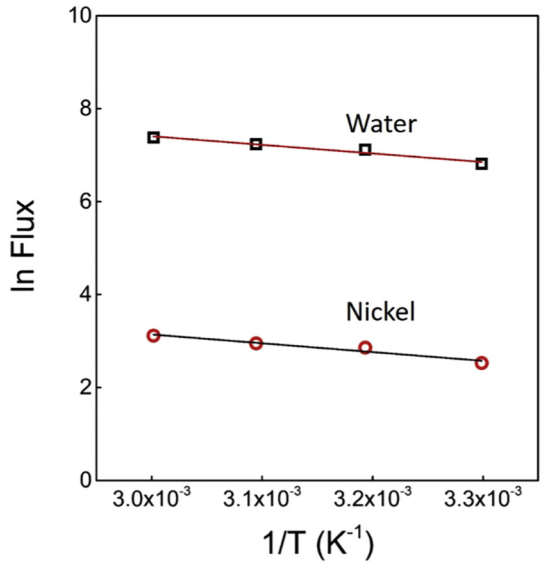

Fig. 8. Arrhenius plot of evaporation of water and percrystallisation of nickel sulphate, using a carbon membrane dip coated in 20 wt% sucrose solution and a feed nickel concentration of 40 g L^{-1}.

concentrations (40 and 50 wt%). These membranes had the lowest water fluxes (Fig. 5). As the vacuum pressure was constant on the permeate side of the membrane during testing, this means that the increase in the sucrose concentration in the carbonised membrane increased the resistance to solution diffusion from feed to permeate side. As less water was available for the production of crystals with the heptahydrate phase, hexahydrate crystals were also formed during percrystallisation. In a similar fashion, the hexahydrate phase was also formed for feed solutions of nickel feed concentration of 100 g L^{-1}, again accompanied by lower water evaporation (Fig. 6).

Crystal morphological studies by SEM imaging show differences between the pure heptahydrate (Fig. 10a) and mixed hepta/hexahydrate (Fig. 10b) crystals. The pure nickel sulphate heptahydrate salts are generally elongated and laminar crystal particles, forming aggregates with sizes of ~200 μm. The samples containing nickel sulphate hepta/hexahydrate mixtures resulted in particles with morphological features that result in a spherical shape (also ~200 μm) with cavities, suggesting imperfections in the growth of the crystals or crystal agglomeration. These findings show that there is a relationship between the morphology of the produced particles which is associated with the diffusion of solution from the feed to the permeate side and the resultant hydration state of the crystals.

From a chemical equilibrium point of view, nickel sulphate heptahydrate is favoured over hexahydrate at temperatures below 28.5 °C considering Eq. 1 at standard conditions with data from HSC Chemistry Software v7.11 (2011). On the permeate side of the membrane, where nickel sulphate hydrate is being crystallised, the temperature is lowered due to the endothermic evaporation of water which favours heptahydrate. However, the presence of a strong vacuum would drive the reaction to the right and favour hexahydrate by promoting water evaporation based on Le Chatelier's principle. From these experiments, our results suggest that the percrystallisation mechanism based on the chemical equilibrium considerations alone as nickel sulphate heptahydrate may have formed preferentially due to the fast reaction kinetics at the wet thin-film interface.

$$NiSO_4 * 7H_2O = NiSO_4 * 6H_2O + H_2O(l) \quad (1)$$

4. Conclusions

This work demonstrates how carbon membrane percrystallisation is a promising technology for hydrometallurgical applications. By tuning the carbon morphological features of the membrane and nickel process conditions, it was possible to attain products with differing hydration states and shapes. On one hand, pure nickel sulphate heptahydrate with elongated and laminar crystal particles (~200 μm) were obtained by using membranes generating high fluxes. On the other hand, a mix of heptahydrate and hexahydrate salts with approximate spherical particles (also ~200 μm) were produced by low flux membranes. Aspect of the reaction pathway, kinetic and equilibrium factors were discussed.

The highest flux obtained for nickel was 1 kg m^{-2} h^{-1} (40 g L^{-1}) with an added benefit of water recovery of 22 L m^{-2} h^{-1}. Solvent recovery is an important aspect in hydrometallurgical processes, particularly to reduce costs and comply with zero liquid discharge environmental regulations. The percrystallisation process also delivered lower activation energy for nickel sulphate crystallisation was estimated at approximately 16 kJ mol^{-1}, lower activation energy than other conventional crystallisation technologies. In summary, inorganic membrane percrystallisation is a novel process with desirable qualities, which may be suited to diverse set of possible applications in hydrometallurgy.

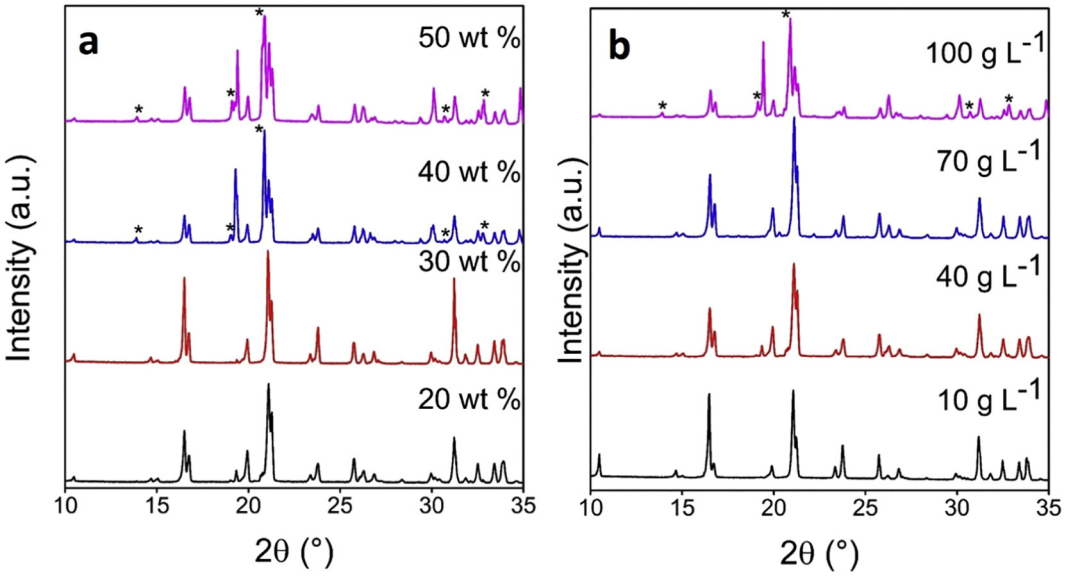

Fig. 9. (a) XRD patterns of nickel sulphate crystals from feed solutions at 40 °C produced by (a) the carbon membranes prepared with various sucrose concentrations with 40 g L^{-1} Ni in feed and (b) the 20 wt% carbon membrane with various nickel feed concentration. Peaks assigned to nickel sulphate hexahydrate are noted by * and are summarised by 2θ = 13.9, 19.1, 20.9, 30.7 and 32.8. XRD files for nickel sulphate hexadydrate (PDF 01-075-0364) and heptahydrate (PDF 01-077-0681).

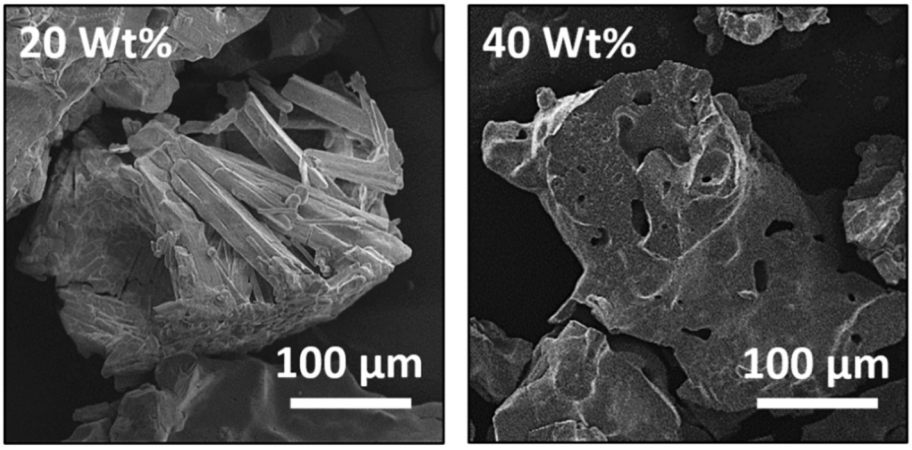

Fig. 10. SEM images of percrystallised samples (a) pure heptahydrate crystal phase produced by a 20 wt% sucrose derived carbon membrane and (b) hexahydrate and heptahydrate phase produced by a carbon membrane using 40 wt% sucrose solution. Testing conditions at 40 °C and a feed nickel concentration of 40 g L^{-1}.

Acknowledgement

The authors acknowledge the financial support for this research from the Australian Research Council (ARC) Discovery Project Grant (DP140102800 and DP190102502). J. C. Diniz da Costa gratefully thanks the support given by the ARC Future Fellowship Program (FT130100405) and the French "Centre National de la Recherche Scientifique" (CNRS-INC section 15) for a 1 month grant as invited Professor at the IEM in Montpellier in 2017.

References

Abd Jalil, S.N., Wang, D.K., Yacou, C., Motuzas, J., Smart, S., Diniz da Costa, J.C., 2017. Vacuum-assisted tailoring of pore structures of phenolic resin derived carbon membranes. J. Membr. Sci. 525, 240–248.

Bamforth, A.W., Crystallizers, Evaporator, 1965a. In: Bamforth, A.W. (Ed.), Industrial Crystallization. L. Hill, London, pp. 98–127.

Bamforth, A.W., Crystallizers, Cooling, 1965b. In: Bamforth, A.W. (Ed.), Industrial Crystallization. L. Hill, London, pp. 31–59.

Beckmann, W., 2013. Crystallization Basic Concepts and Industrial Applications. John Wiley & Sons, pp. 173–185.

Chen, G., Lu, Y., Krantz, W.B., Wang, R., Fane, A.G., 2014. Optimization of operating conditions for a continuous membrane distillation crystallization process with zero salty water discharge. J. Membr. Sci. 450, 1–11.

Curcio, E., Simone, S., Profio, G.D., Drioli, E., Cassetta, A., Lamba, D., 2005. Membrane crystallization of lysozyme under forced solution flow. J. Membr. Sci. 257, 134–143.

Dimaras, P.I., 1956. Morphology and structure of anhydrous nickel sulphate. Acta Crystallogr. 10, 313–315.

Elma, M., Wang, D.K., Yacou, C., Diniz da Costa, J.C., 2015. Interlayer-free P123 carbonised template silica membranes for desalination with reduced salt concentration polarisation. J. Membr. Sci. 475, 376–383.

Feng, X., Huang, Y.M., 1996. Estimation of activation energy for permeation in pervaporation process. J. Membr. Sci. 118, 127–131.

GME, 2015–2018. Nickel market outlook, in: G.R. Limited (Ed.), GME Resource Limited. http://www.gmeresources.com.au/nickel-market-outlook.php.

Gong, C., Zhao, L., Li, S., Wang, H., Gong, Y., Wang, R., He, B., 2018. Atomic layered deposition iron oxide on perovskite $LaNiO_3$ as an efficient and robust bi-functional catalyst for lithium oxygen batteries. Electrochim. Acta 281, 338–347.

Government of South Australia, Department of the Premier and Cabinet Minerals, Geoscience, Salt. http://minerals.statedevelopment.sa.gov.au/invest/mineral_commodities/salt, Accessed date: 23 September 2018.

Hasan, M., Louhi-Kultanen, M., 2016. Water purification of aqueous nickel sulfate solutions by air cooled natural freezing. Chem. Eng. J. 294, 176–184.

Havlik, T., Skrobian, M., Kammel, R., Curilla, J., Cmorejova, D., 1996. Refining crude nickel sulphate obtained from copper electrolyte. Hydrometallurgy 79–88.

Hewitson, C., 2017. The Lion salt works, Northwich: a legacy of the Cheshires industry. Ind. Archaeol. Rev. 39, 59–75.

Huang, B., Liu, Q., Caro, J., Huang, A., 2014. Iso-butanol dehydration by pervaporation using zeolite LTA membranes prepared on 3-aminopropyltriethoxysilane-modified alumina tubes. J. Membr. Sci. 455, 200–206.

INSG, 2018. In: I.N.S. Group (Ed.), Production, Usage and Prices. International Nickel Study Group. http://www.insg.org/prodnickel.aspx.
Ji, X., Curcio, E., Al Obaidani, S., Di Profio, G., Fontananova, E., Drioli, E., 2010. Membrane distillation-crystallization of seawater reverse osmosis brines. Sep. Purif. Technol. 71, 76–82.
Kornev, K.G., Neimark, A.V., 2001. Spontaneous penetration of liquids into capillaries and porous membranes revisited. J. Colloid Interface Sci. 235, 101–113.
Lamiel, C., Nguyen, V.H., Hussain, I., Shim, J.-J., 2017. Enhancement of electrochemical performance of nickel cobalt layered double hydroxide@nickel foam with potassium ferricyanide auxiliary electrolyte. Energy 140, 901–911.
Lascelles, K., Morgan, L.G., Nicholls, D., Beyersmann, D., 2005. Nickel Compounds. In: Ullmann's Encyclopedia of Industrial Chemistry. Wiley-VCH, Weinheim. https://doi.org/10.1002/14356007.
Lee, J., Wu, Y., Peng, Z., 2018. Hetero-nanostructured materials for high-power lithium ion batteries. J. Colloid Interface Sci. 529, 505–519.
Lei, Y., Li, J., Wang, Y., Gu, L., Chang, Y., Yuan, H., Xiao, D., 2014. Rapid microwave-assisted green synthesis of 3D hierarchical flower-shaped NiCo(2)O(4) microsphere for high-performance supercapacitor. ACS Appl. Mater. Interfaces 6, 1773–1780.
Liang, B., Zhan, W., Qi, G., Lin, S., Nan, Q., Liu, Y., Cao, B., Pan, K., 2015. High performance graphene oxide/polyacrylonitrile composite pervaporation membranes for desalination applications. J. Mater. Chem. A 3, 5140–5147.
Madsen, R.S.K., Motuzas, J., Julbe, A., Diniz da Costa, J.C., 2018. Fine control of NaCl crystal size and particle size in percrystallisation by tuning the morphology of carbonised sucrose membranes. J. Membr. Sci. 567, 157–165.
Mariah, L., Buckley, C.A., Brouckaert, C.J., Curcio, E., Drioli, E., Jaganyi, D., Ramjugernath, D., 2006. Membrane distillation of concentrated brines – role of water activities in the evaluation of driving force. J. Membr. Sci. 280, 937–947.
Moldoveanu, G.A., Demopoulos, G.P., 2002. Producing high-grade nickel sulfate with solvent displacement crystallization. J. Miner. Metals Mater. Soc. (TMS) 54, 49–53.
Mortimer, M., Taylor, P., Clark, G., Smart, L.E., 2002. Reactions in solution. In: Mortimer, M., Taylor, P. (Eds.), Chemical Kinetics and Mechanism. Royal Society of Chemistry, pp. 80–91.
Motuzas, J., Yacou, C., Madsen, R.S.K., Fu, W., Wang, D.K., Julbe, A., Vaughan, J., Diniz da Costa, J.C., 2018. Novel inorganic membrane for the percrystallization of mineral, food and pharmaceutical compounds. J. Membr. Sci. 550, 407–415.
Oh, Y.J., Kim, J.H., Park, S.-K., Park, J.-S., Lee, J.-K., Kang, Y.C., 2018. Highly efficient hierarchical multiroom-structured molybdenum carbide/carbon composite microspheres grafted with nickel-nanoparticle-embedded nitrogen-doped carbon nanotubes as air electrode for lithium-oxygen batteries. Chem. Eng. J. 351, 886–896.
Olivier, M.C., Dorfling, C., Eksteen, J.J., 2012. Evaluating a solvent extraction process route incorporating nickel preloading of Cyanex 272 for the removal of cobalt and iron from nickel sulphate solutions. Miner. Eng. 27, 37–51.
Peng, P., Fane, A.G., Li, X., 2005. Desalination by membrane distillation adopting a hydrophilic membrane. Desalination 173, 45–54.
Phillips, V.R., Epstein, N.S., 1974. Growth of nickel sulfate in a laboratory-scale fluidized-bed crystallizer. AICHE J. 20, 678–687.
Pilling, M.J., Seakins, P.W., 1999. Diffusion-controlled reactions. In: Pilling, M.J., Seakins, P.W. (Eds.), Reaction Kinetics. Oxford University Press, United Kingdom, pp. 151.
Polino, M., Carvalho, A.L.S., Juknaitė, L., Portugal, C.A.M., Coelhoso, I.M., Romão, M.J., Crespo, J.G., 2017. Ion-exchange membranes for stable derivatization of protein crystals. Cryst. Growth Des. 17, 4563–4572.
Prasad, K.V.R., Ristic, R.I., Sheen, D.B., Sherwood, J.N., 2000. Crystallization of paracetamol from solutions in the presence and absence of impurity. Int. J. Pharm. 215, 29–44.
Quist-Jensen, C.A., Ali, A., Mondal, S., Macedonio, F., Drioli, E., 2016. A study of membrane distillation and crystallization for lithium recovery from high-concentrated aqueous solutions. J. Membr. Sci. 505, 167–173.
Quist-Jensen, C.A., Sørensen, J.M., Svenstrup, A., Scarpa, L., Carlsen, T.S., Jensen, H.C., Wybrandt, L., Christensen, M.L., 2018. Membrane crystallization for phosphorus recovery and ammonia stripping from reject water from sludge dewatering process. Desalination 440, 156–160.
Sarti, G.C., Gostoli, C., Matulli, S., 1985. Low energy cost desalination processes using hydrophobic membrane. desalination 56, 277–286.
Semiat, R., 2008. Energy issues in iesalination processes. Environ. Sci. Technol. 8193–8201.
Su, C., Puls, R.W., 1999. Kinetics of trichloroethene reduction by zerovalent iron and tin: pretreatment effect, apparent activation energy, and intermediate products. Environ. Sci. Technol. 33, 163–168.
Tsai, J.-H., Macedonio, F., Drioli, E., Giorno, L., Chou, C.-Y., Hu, F.-C., Li, C.-L., Chuang, C.-J., Tung, K.-L., 2017. Membrane-based zero liquid discharge: myth or reality? J. Taiwan Inst. Chem. Eng. 80, 192–202.
Tun, C.M., Fane, A.G., Matheickal, J.T., Sheikholeslami, R., 2005. Membrane distillation crystallization of concentrated salts—flux and crystal formation. J. Membr. Sci. 257, 144–155.
Varnavas, S.P., Lekkas, T., 1996. Factors controlling the geochemical and crystallization processes in marine brine ponds. Mar. Geores. Geotechnol. 14, 111–141.
Wang, N., Sun, B., Zhao, P., Yao, M., Hu, W., Komarneni, S., 2018. Electrodeposition preparation of $NiCo_2O_4$ mesoporous film on ultrafine nickel wire for flexible asymmetric supercapacitors. Chem. Eng. J. 345, 31–38.
Weschenfelder, T.A., Lantin, P., Viegas, M.C., de Castilhos, F., Scheer, A.d.P., 2015. Concentration of aroma compounds from an industrial solution of soluble coffee by pervaporation process. J. Food Eng. 159, 57–65.
Xiong, G., He, P., Liu, L., Chen, T., Fisher, T.S., 2015. Plasma-grown graphene petals templating Ni–Co–Mn hydroxide nanoneedles for high-rate and long-cycle-life pseudocapacitive electrodes. J. Mater. Chem. A 3, 22940–22948.
Xu, K., Feng, B., Zhou, C., Huang, A., 2016. Synthesis of highly stable graphene oxide membranes on polydopamine functionalized supports for seawater desalination. Chem. Eng. Sci. 146, 159–165.
Ye, W., Lin, J., Shen, J., Luis, P., Van der Bruggen, B., 2013. Membrane crystallization of sodium carbonate for carbon dioxide recovery: effect of impurities on the crystal morphology. Cryst. Growth Des. 13, 2362–2372.
Zhang, H., Wang, Y., 2016. Poly(vinyl alcohol)/ZIF-8-NH_2 mixed matrix membranes for ethanol dehydration via pervaporation. AICHE J. 62, 1728–1739.
Zhao, T., Gao, X., Wei, Z., Guo, K., Wu, F., Li, L., Chen, R., 2018. Three-dimensional $Li_{1.2}Ni_{0.2}Mn_{0.6}O_2$ cathode materials synthesized by a novel hydrothermal method for lithium-ion batteries. J. Alloys Compound. 757, 16–23.